High Accuracy Pointing for Quasi-optical THz Mixer Arrays

Gasparsilva, Jose Rui; Finkel, Matvey; Laauwen, Wouter; Westerweld, Menno; More, Nikhil; Young, Abram; Kulesa, Craig; Walker, Christopher; Van der Tak, Floris; Gao, Jian Rong

DOI
10.1109/TTHZ.2021.3118607

Publication date
2022

Document Version
Accepted author manuscript

Published in
IEEE Transactions on Terahertz Science and Technology

High Accuracy Pointing for Quasi-optical THz Mixer Arrays

José R.G. Silva, Matvey Finkel, Wouter M. Laauwen, Menno Westerweld, Nikhil More, Abram Young, Craig Kulesa, Christopher Walker, Floris van der Tak, and Jian Rong Gao

***Abstract*— We report a high accuracy pointing technique for quasi-optical hot electron bolometer (HEB) mixers in focal-plane arrays designed to operate at 1.4, 1.9 and 4.7 THz. The high accuracy pointing is achieved by pre-alignment of a HEB chip to a lens, measuring the angular error of each mixer in an array assembly, and then re-alignment of the chip to the same lens to correct the error. The re-aligned mixers, using 5 mm diameter Si elliptical lenses designed for operation at 4.7 THz, show a final pointing error distribution with an average (μ) = 0.13 deg and standard deviation (σ) = 0.06 deg, with respect to the normal direction of the respective array plane. Those using 10 mm diameter lenses designed for operation either at 1.4 or 1.9 THz, show μ = 0.08 deg and σ = 0.03 deg. We demonstrated our pointing technique in five 4×2 HEB focal plane arrays developed for NASA's balloon borne GUSTO THz observatory. Our results corroborate the simulated beam steering factors used to calculate the re-alignment corrections. With the unprecedented pointing accuracy at the high frequencies, our technique can significantly facilitate the use of lens-antenna, quasi optical mixers for future focal-plane arrays, which is able to compete with traditional feedhorn-waveguide mixer arrays, operated typically below 1 THz, for astronomical instrumentation.**

***Index Terms*— Antenna radiation pattern, antenna arrays, beam steering, cryogenic, lenses, terahertz radiation.**

I. Introduction

TERAHERTZ heterodyne receivers, ranging roughly from 0.1 to 6 THz, have been used extensively for astronomy due to their extremely high spectral resolution capabilities (R~10^7) [1]. With such systems it is possible to observe astronomically important atomic fine-structure and molecular rotational lines that are abundant in this frequency range. Using these lines as tracers it is possible to understand the dynamics and chemical processes within star forming regions [2], [3]. Moreover, THz heterodyne receivers due to their coherent nature also offer great interferometry possibilities that, for example, are key to study the physics of the event horizon of supermassive black holes [4].

A heterodyne receiver consists of a mixer element that multiplies an unknown celestial signal with a much stronger and known signal from a local oscillator (LO), generating a copy of the former at the frequency of the difference between the two signals, which is the so-called intermediate frequency (IF). Between 1 and 6 THz, the heterodyne receiver uses typically a superconducting niobium nitride (NbN) Hot Electron Bolometer (HEB) mixer since it is currently the most sensitive heterodyne detector available in this frequency range [5]. As local oscillators, different coherent source types, solid-state sources based on a multiplier-chain at frequencies below 2 THz [6] or quantum cascade lasers (QCLs) above 2 THz [7][8], can be used. Because the sensitivity of current HEB mixers is approaching the quantum noise limit [9] there is a need to develop multi-pixel array receivers in order to improve mapping speeds of future instruments. Recent important technology improvements, such as high power QCLs [10], [11] and LO multiplexing schemes based on a Fourier phase grating [12], offer solutions to fulfill the existing demands for multi-pixel THz heterodyne systems for airborne [13], balloon borne [14], [15] and possibly future space [16] THz observatories.

The most common radiation coupling schemes for THz mixers are either quasi-optical, namely lens-antenna, or feedhorn-waveguide. At the frequencies above 2 THz, it is both challenging and expensive to manufacture good quality waveguide structures due to the reduced feature size [17], which is not the case for quasi-optical schemes that are easily manufacturable. Therefore, the latter offers a good solution to scale the number of pixels in receivers at those frequencies. However, quasi-optical schemes are known to be difficult in achieving high accuracy pointing of the far-field beams since they require the use of an alignment method for the antenna of a mixer to the optical axis of a lens that is challenging to obtain

This paragraph of the first footnote will contain the date on which you submitted your paper for review. This work was supported in part by the National Aeronautics and Space Administration (NASA)'s GUSTO funding through the University of Arizona and EU Horizon 2020 RadioNet. (Corresponding author: Jose R. G. Silva).

J. R. G. Silva and F. Van Der Tak are with the SRON Netherlands Institute for Space Research, Landleven 12, 9747 AD. Groningen, The Netherlands, and also with the Kapteyn Astronomical Institute, University of Groningen, Landleven 12, 9747 AD, Groningen, The Netherlands (e-mail: j.r.g.d.silva@sron.nl; F.F.S.van.der.Tak@sron.nl)

M. Finkel, W. M. Laauwen, M. Westerweld and N. More are with the SRON Netherlands Institute for Space Research, Landleven 12, 9747 AD. Groningen, The Netherlands (e-mail: m.finkel@gmail.com; W.M.Laauwen@sron.nl; M.J.Westerveld@sron.nl; nmore@mpe.mpg.de)

A. Young, C. Kulesa, and C. Walker are with the Steward Observatory, 933 N Cherry Ave., Rm N204, University of Arizona, Tucson, Arizona 85721, USA (e-mail: young@physics.arizona.edu; ckulesa@arizona.edu; iras16293@gmail.com)

J. R. Gao is with the SRON Netherlands Institute for Space Research, Niels Bohrweg 4, 2333 CA, Leiden, and also with Optics Research Group, Imaging Physics department, Delft University of Technology, The Netherlands (e-mail: j.r.gao@sron.nl)

This article has been accepted for publication in a future issue of this journal, but has not been fully edited. Content may change prior to final publication. Citation information: DOI 10.1109/TTHZ.2021.3118607, IEEE Transactions on Terahertz Science and Technology

micrometer-level accuracy. A non-ideal alignment also contributes to create beam squint that is not desired [18].

GUSTO is a NASA ultra-long duration balloon borne terahertz observatory [15] that will employ three focal-plane arrays based on quasi-optical HEB mixers to simultaneously measure the fine structure lines of [NII], [CII] and [OI] at 1.4, 1.9 and 4.7 THz, respectively. It requires the use of compact focal-plane arrays, each of which consists of 8 pixels in a 4×2 configuration. GUSTO array's architecture takes a different approach compared to the mixer arrays employed in the upGREAT instrument [13], which consist of multiple individual mixers that can have their THz far-field beams independently aligned. GUSTO's approach has the advantage of a reduced footprint of the array and coupling optics in the instrument. However, it requires high accuracy pointing of the beams of all the pixels to ensure their co-alignment, and therefore, parallel propagation in the telescope optical system. This is crucial to reduce optical spillover, e.g., through the secondary mirror of the Cassegrain telescope, which can reduce the mapping efficiency. Furthermore, it is important for the beam matching to the LOs since any angular offsets between two gaussian beams can reduce the coupling efficiency. Ideally also all the mixers should receive not only sufficient but also equal LO power. The LOs at 1.4 THz and 1.9 THz are based on an array of sources made of multiplier chains, which allow to tune the output power individually. Therefore, the pointing for the lower frequency arrays is less critical as far as the coupling to the LO is concerned. However, the 4.7 THz LO makes use of a Fourier phase grating [12] to generate an array of LO beams from a single QCL, which does not allow for adjusting the power of the beams individually. Thus, the high accuracy pointing becomes crucial with respect to coupling LO beams. GUSTO requires the pointing error of each pixel within an array to be below 0.1 degree relative to the normal direction of the array plane. With this requirement it is guaranteed that all focal plane array beams properly illuminate the telescope, achieving higher than 95% telescope aperture efficiency, especially the corner pixels of the array. This number is a factor of 3 smaller than what was defined for single pixel mixers for Band 6 and 7 in the HIFI instrument on board of The Herschel Space Observatory [19][20], the only example found on quasi-optical receivers operated at THz frequencies in the literature. In a case by case basis, GUSTO's pointing requirement could be relaxed up to 0.2 or in some cases 0.3 degrees if the pixel final pointing direction is directed towards the center of the optical system, and the coupling to the LO is similar to the other pixels in the array. To meet this requirement the easiest solution would be to use extra optics in front of each mixer in the array, similar to HIFI, however, with multiple arrays this would lead to a too complex system to be implemented for a space-like instrument. As a solution, we propose to align each mixer twice, by measuring the pointing of each pixel in the array after the first alignment of a HEB detector to a lens, and then re-align to correct the measured angular offset. With this approach we have realized arrays of 8 pixels, which either meet or approach the GUSTO pointing requirement.

This paper reports a technique to realize and characterize the far-field beam pointing of quasi-optical mixers and, in particular, their focal-plane arrays with an unprecedented accuracy in the frequency range between 1 and 6 THz. We start by introducing our lens-antenna mixer configuration and the main contributors to the pointing error. Thereafter we describe the methodology used to obtain highly reproducible alignments of an HEB chip on a lens, with ±2 μm accuracy to the targeted position. We also describe the mixer pointing measurement setup that has an uncertainty within ±0.03 degrees. We report the implementation of such a technique in the realization of five mixer arrays for GUSTO, which use Si elliptical lenses with two different diameters.

II. High accuracy pointing technique

A. Lens-antenna system and expected pointing error

Each mixer consists of a NbN HEB integrated with a planar, tight winding spiral antenna, both fabricated on a Si chip and shown in Fig. 1 (a). The HEB is 2μm in width, 0.15μm in length and 5nm in thickness. The antenna is designed as in [21], details can be found in [22]. The HEB chip is then mounted on a Si elliptical lens. Both the chip and lens are made of pure, highly resistive Si.

Fig.1 (b) illustrates the elliptical lens design [23], where "a" is the ellipse major axis, "b" the ellipse minor axis, also referred as lens radius, and "c" the extension length. Two different lens diameters are used in our work: 5 mm diameter lenses, with a major axis of 2617μm and an extension length matching the focal distance of 775μm, which will be referred as the small lenses, for the mixers to be operated at 4.7 THz; and 10 mm diameter lenses, hereon referred as the large lenses, with 5235μm major axis, and an extension length of 1550 μm, matching the focal distance, and 1535 μm for the mixers to be operated at 1.4 and 1.9 THz, respectively. The extension length difference in the 10 mm diameter lenses is small enough that can be ignored for the purpose of our pointing corrections.

Fig. 1 (c) illustrates how a HEB chip is aligned and glued to the backside of a lens. To form an array, each is then transferred

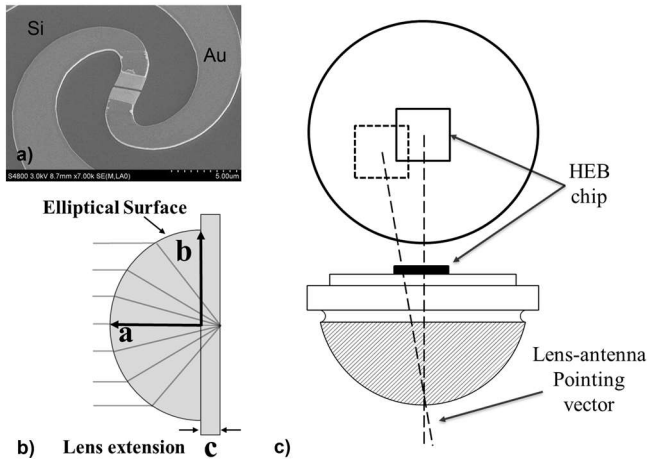

Fig. 1 SEM micrograph of a tight winding spiral antenna coupled HEB mixer, where the HEB locates at the center of the antenna; b) Elliptical lens design; c) Alignment schematic with pointing vector for the combination of a HEB chip and a Si lens.

This article has been accepted for publication in a future issue of this journal, but has not been fully edited. Content may change prior to final publication. Citation information: DOI 10.1109/TTHZ.2021.3118607, IEEE Transactions on Terahertz Science and Technology

into an array mixer block for the final assembly. In this work, we will focus on the pointing error of each individual mixer in the final assembly, where in the ideal case all the beams from the mixers should propagate perpendicularly to the array plane into the far field.

We expect three main contributors to the pointing error of a pixel in the final array. The first is the alignment of a HEB chip to a lens, which is referred to Fig 1(c). Specifically, this is the alignment between the center of the spiral antenna, where the NbN bolometer is located, and the center of the back surface of the lens, where the optical axis is assumed. To understand the impact of this contributor we performed finite element analysis using the high frequency structure simulator, HFSS [24], and a combination of geometric and physical optics to simulate different misalignments between the antenna and the optical axis for both small and large lenses [25]. From the simulations we found a beam steering factor, representing the misalignment sensitivity, of ≈0.066 deg/μm relative to the lens optical axis for the small lenses. For the large lenses we obtained ≈0.033 deg/μm. The second contributor is the manufacturing tolerance of the Si lenses, that can impact the exact position of the optical axis in the back surface of a lens. For example, considering the concentricity of the back surface to the front elliptical surface, the tolerance is ±5 μm. This uncertainty has the same impact on the pointing as the first contributor, which would give an uncertainty within ±0.33 deg for the small lenses even if the antenna would be perfectly centered on the back surface. The third contributor is the combination of all machining tolerances of the array mixer block assembly. Examples of these tolerances are the degree of perpendicularity between the pocket surface, where the lenses are placed, and the array normal, and how flat these pockets are. The pointing errors originated from these tolerances stack with the previous errors. This contribution was designed to be ± 0.02 deg, which is smaller in comparison with the other two. We conclude that achieving a pointing error smaller than 0.1 deg for all the pixels in an array requires not only an accurate alignment of a HEB chip to a lens, but also a step where we characterize the pointing error of each pixel, which will include the error contributions from the three sources, followed by the re-alignment of the chip to a new position that cancels the measured pointing error.

B. *Lens-antenna alignment method*

Our method to align an antenna on a chip to a lens can be summarized in the following steps: a) pre-align a HEB chip on the back of a lens; b) measure pointing error of the pixel in the final array assembly relative to a desired reference, which in our case is the normal direction to the array plane; c) calculate the corrections for the HEB antenna position based on the measured error, using the lens's simulated beam steering factor; d) re-align the HEB chip to the new position on the lens; f) re-measure the pointing of the same pixel. The same procedure applies to all the mixers (pixels) in the array. Further details are available in Appendix A.

Because this method relies on the re-alignment of the chip in step c), it requires the assembly of the mixer block to be highly reproducible, where the lens orientation relative to the normal direction of the array must always be the same. With this requirement we ensure that only the chip re-alignment causes a change in the pointing. Furthermore, using this method it is possible to correct for any pointing error above its accuracy."

C. *Pointing measurement setup*

Fig. 2 illustrates a detailed schematic of the pointing measurement setup with side and top views in (a) and (b), respectively; the cryostat front in (c), and an array mounted on the cold plate of the cryostat in (d). To characterize the pointing of each pixel we measure its two-dimensional, XY, far-field beam patterns at different Z-axis positions. From these beam patterns we calculate the pointing angle relative to the normal direction of the array plane. The beam patterns are obtained by measuring the current response of the HEB operated in direct detector mode to a movable THz source as a function of the source XY position. The THz source used is a glow bar, IR-Si207 source from Hawk Eye Technologies, assembled in a setup similar to the one used in [26], mounted on a high precision XYZ stage, 3 axis 8MT295 Series from Standa, that scans the glow bar in front of the cryostat, where the HEB is mounted. The glow bar signal is chopped at a frequency of 38 Hz. The observable is the AC current response of the HEB, which is acquired by a lock-in amplifier. The beam patterns are measured at three different distances away from the HEB.

Since the glow bar emits wideband THz radiation and the HEB is operated in direct detection mode, the measured beam

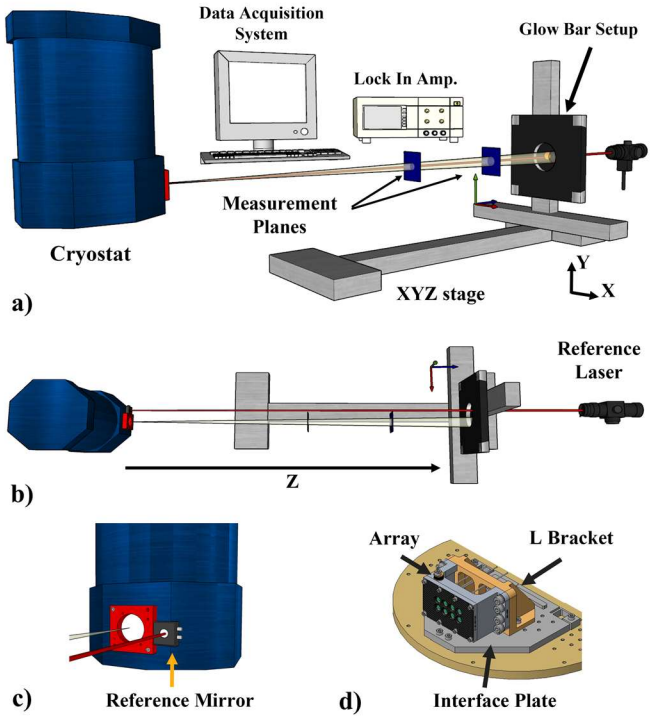

Fig. 2 Beam pointing measurement setup. a) and b) side and top view, respectively. The HEB mixer array is cooled to a liquid helium temperature inside the cryostat and operated at its resistive transition. The glow bar source mounted on the XYZ stage is chopped at a frequency of 38 Hz and scanned in front of the cryostat at different planes. The lock-in amplifier measures the AC current response of the HEB. The reference laser is used to align the cryostat to the setup by reflecting the light on the cryostat's reference mirror back to the laser. c) Front view of the cryostat with reference mirror mounted. d) Inside view of the cryostat. The HEB mixer array is mounted on a L-bracket that is placed on the interface plate assembled on the cryostat cold plate.

This article has been accepted for publication in a future issue of this journal, but has not been fully edited. Content may change prior to final publication. Citation information: DOI 10.1109/TTHZ.2021.3118607, IEEE Transactions on Terahertz Science and Technology

pattern contains a superposition of all the beam patterns at different frequencies and is thus wideband. We found this superposition to be consistently highly gaussian, >99%, and therefore highly reliable and reproducible to determine the coordinates of the wideband beam center, which is a parameter of the 2D gaussian profile to be fit to a measured intensity pattern. Furthermore, we have also simulated the beam steering effect for a misalignment between the antenna and the optical axis of a small lens at either 1.4 or 5.3 THz [25]. From the simulations we found that for a 30 μm misalignment, which is a much higher value than an expected misalignment error, the angular difference between both frequencies is below 0.02 deg, or 1% error. Moreover, the error will be smaller because of the smaller misalignments in practice. Therefore, we conclude that for the expected pointing errors, the pointing of the mixer determined from the wideband beam patterns is representative of any frequency within the antenna bandwidth, and thus, our methodology is valid to achieve a high pointing accuracy at the frequencies of our interest.

Assuming a small angle regime, the pointing error, θ, is calculated using (1), where dx/dz and dy/dz represent the fitted slope of the beam center displacement as a function of the distance, for the horizontal and vertical coordinates respectively, after correcting for the systematic pointing error of the measurement system as will be discussed later in this paper.

$$\theta = \sqrt{\left(\tan^{-1}\left(\frac{dx}{dz}\right)\right)^2 + \left(\tan^{-1}\left(\frac{dy}{dz}\right)\right)^2} \quad (1)$$

We are interested in the pointing error of the mixers within an array with respect to the array normal. Therefore, the Z-axis of the stage, see Fig. 2(b), has to be aligned to this direction. However, the array is mounted inside a cryostat with a QMC heat filter, that filters the radiation above 6 THz, while the spiral antenna has the lower cut-off frequency of about 0.5 THz in our case, and ultra-high molecular weight polyethylene (UHMWPE) window. Both are transparent at THz frequencies, but opaque to visible light, making it impossible to perform a direct alignment to the normal of the array. To overcome this, we replicate the normal of the array with a flat mirror assembled on the outside of the cryostat as shown in Fig. 2(c), where it is accessible. This mirror is then aligned to a reference laser of visible light that was pre-aligned to the Z-axis of the stage. In this way we can align the stage Z-axis to the normal of the array. In the next paragraphs we will discuss the pre-calibrations required for the orientation of the flat reference mirror and the reference laser and also the final calibration measurements to determine and correct the systematic error due to them.

The array block, where eight HEB mixers are assembled, is first screwed onto a L-shaped bracket. The latter is mounted on an interface plate, as shown in Fig. 2(d). All these are made of Al. The interface plate is introduced to compensate the mismatch in thermal expansion between the Al array block and the Cu cold plate of the cryostat. Per design, the array and the L-bracket have the same normal direction. Note that in this case the errors due to machining were found to be negligible. To calibrate the normal of the array, we replace the array with a flat mirror on the L bracket, remove the heat filter, replace the UHMWPE window with a mylar window and also cool the cryostat down to a liquid helium temperature. Using a theodolite in position A, as shown in Fig. 3, we measure the back reflection direction from the mirror inside the cryostat, which is the direction of interest. We then replicate the same normal direction on the reference mirror outside the cryostat. The replication is done by moving the theodolite laterally to a new position B, not shown in Fig. 3, so the theodolite faces the reference mirror. While in position B we tune the reference mirror until we replicate the same angular difference, namely $\Delta\theta_A = \Delta\theta_B$, between both mirrors, inside and outside the cryostat, and the setup reference mirror, also included in Fig. 3.

The second required angular calibration is the reference laser to the Z-axis of the stage. Here we place a camera, DCC1645C

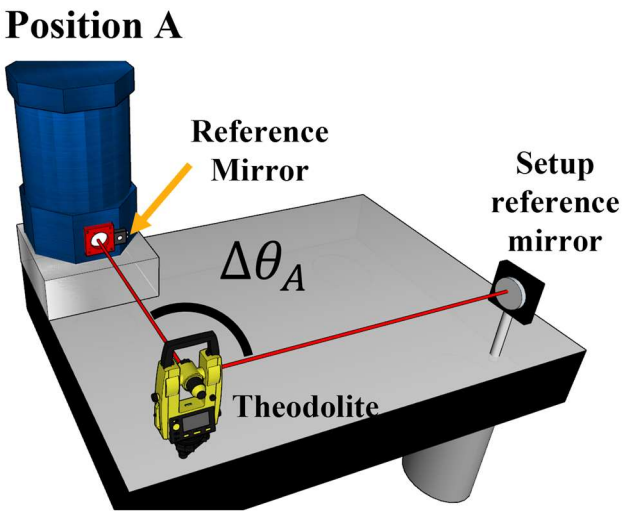

Fig. 3. Setup for the replication of the normal direction of an array. Theodolite shown in position A where it faces the mirror inside the cryostat. The reference mirror on the cryostat is adjusted so that its orientation verifies the condition $\Delta\theta_A = \Delta\theta_B$, effectively copying the normal direction of the array. $\Delta\theta_B$ is the angle between the reference mirror and the setup reference mirror, not shown. [27]

from Thor labs, on the back of the glow bar unit and make the laser light emit towards it. By moving the stage within the available range on the Z-axis it is possible to detect the direction mismatch between the laser and the Z-axis by looking at the laser displacement on the camera. With the reference laser adapted with tip/tilt and translation micrometer stages, we correct the laser beam direction to match the stage movement. For verification, we take images with the camera in 6 different XY planes along the Z-axis. For each we find the laser beam center position by fitting, and calculate the angular offset using (1). We are able to achieve alignments of the laser to the stage within an error of 0.02 degrees.

To perform a pointing measurement of a mixer, the array will replace the mirror inside the cryostat, while the heat filter and UHMWPE window are re-installed. We now rely on the mirror outside the cryostat to reflect the beam of the reference laser back to itself. In this case, we align the back reflected beam to the laser aperture which allows adjusting the cryostat and thus the normal of the array as required.

The final calibration of the setup is performed by first measuring the pointing of multiple pixels with the array mounted as in Fig. 2(d). Subsequently, we measure the pointing again but now with the array rotated by 180 degrees around the

This article has been accepted for publication in a future issue of this journal, but has not been fully edited. Content may change prior to final publication. Citation information: DOI 10.1109/TTHZ.2021.3118607, IEEE Transactions on Terahertz Science and Technology

normal. For each pixel, the average pointing between the two measurements represents the normal of the array relative to the normal direction, Z-axis, of the scanned planes. By averaging the previous values for all the pixels measured we obtain the systematic pointing error of our measurement setup, which includes all the errors mentioned in the previous calibrations. We use the systematic pointing error obtained to correct the fitted slopes for each pixel, which we then use to calculate the final pointing error using (1). The final uncertainty of the pointing is due to the combination of each beam pattern quality and the reference mirror alignment to the reference laser, and is estimated to be ± 0.03 deg.

III. Results and Discussions

A. *Pointing measurements*

We applied the two alignment procedures to determine and correct the pointing of five arrays to realize the required high accuracy pointing. Three arrays use the large lenses and another two use the small lenses. The pointing measurements were performed with the HEBs at 400mm distance from the first scanned plane for the arrays with the small lenses, and 800mm with the large lenses. The second and third planes are at 250 and 500 mm after the first one. The small lenses were measured at the shorter distance to achieve a sufficiently high signal-to-noise ratio since their beams are more divergent. Furthermore, because the signal decreases with the plane distance due to increased atmospheric absorption and beam size, we measured the beam at the second plane twice and at the third plane three times and took the averaged beam at each plane. The finally obtained signal to noise ratio at the beam center was found to be on average 18, 14 and 11 dB for each plane, respectively, with a variation of ±1 dB.

In Fig. 4 we present an example of the pointing measurement results for a re-aligned pixel, P1, using a large lens, where the plots in (a), (b) and (c) are the final measured 2D beam patterns at 800, 1050 and 1300 mm from the mixer, respectively. By fitting these measurements with a 2D Gaussian profile we were able to obtain the beam center position, which is one of the fitting parameters and is marked in the central area of each image. We calculate the beam center displacement in both vertical and horizonal directions relative to the first plane as a function of the distance, as shown in Fig. 4(d). Using a linear least square fit to the data, we derive the pointing offset to be 0.036 ± 0.021 deg in the horizontal direction and -0.058 ± 0.021 deg in the vertical direction relative to the stage Z-axis. Furthermore, we measured another pixel, P2, in the regular orientation and 180 degrees rotated. From the pointing error average of these two orientations, we found the array to have its normal orientation at -0.05 deg in the horizontal direction and -0.02 deg in the vertical direction. Having corrected the P1 measured horizontal and vertical errors for this common offset, we then apply (1) to calculate the final pointing error. In Fig. 4(e) we show a polar plot that summarizes the final pointing direction and the magnitude of the angular error for the above measurements. The final offset for P1 is 0.09 deg, being below the 0.1 deg specification for GUSTO, is an extremely small angular offset and therefore an excellent result. In comparison, before the realignment the same pixel showed a pointing error of 0.46 deg.

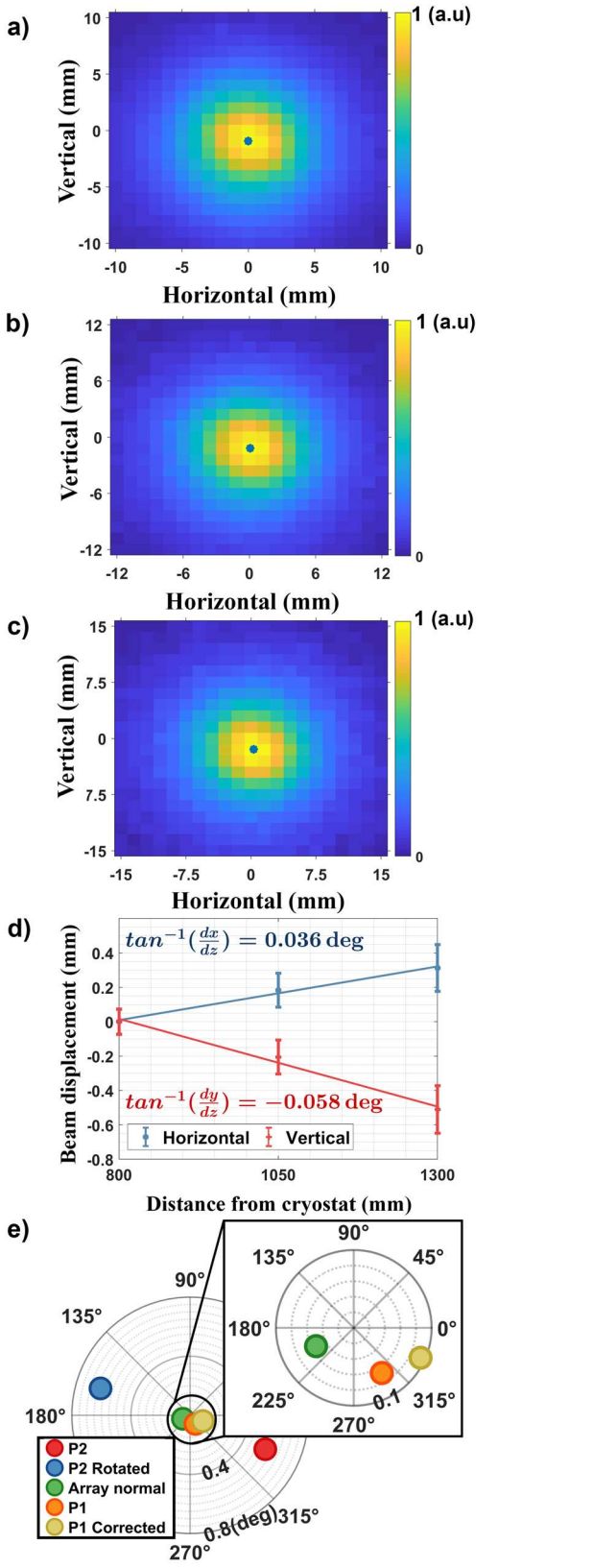

Fig. 4. Pointing measurements for a re-aligned pixel, P1, using a 10 mm diameter lens. (a), (b) and (c) show measured beam patterns at a distance of 800, 1050 and 1300 mm from the mixer, respectively, where fitted beam centers are also indicated. (d) shows beam displacement with fitted slope used to derive the angular offset of the pixel relative to the stage Z-axis. (e) shows different pointing measurements used to obtain the final pointing result for the re-aligned pixel, P1.

This article has been accepted for publication in a future issue of this journal, but has not been fully edited. Content may change prior to final publication. Citation information: DOI 10.1109/TTHZ.2021.3118607, IEEE Transactions on Terahertz Science and Technology

B. *Pointing measurements results of arrays*

We now discuss the pointing measurement results for arrays. Among the 16 pixels using the small lenses, 14 pixels were re-aligned using our method. The other two were found to have undesired mechanical structure in the pocket of the array block where the respective lens was mounted, consisting of a protuberance of a few micrometers. The protuberance causes the two lenses to have different potential orientations when they were assembled on the mixer block, which we could not control. Because of this it is invalidated for us to apply the re-alignment procedure, since our technique requires the lenses to always have the same orientation when assembled on the mixer block. The final error for these two pixels is about 0.3 deg. We note that once fully assembled both pixel orientations are stable. For the large lenses, 19 out of the 24 were re-aligned, while the other five lenses were not re-aligned. The reason is that they have showed a pointing error smaller than 0.2 deg after the pre-alignment, found to have a limited impact on the instrument performance despite being out of the specification. Thus, we decide not to perform the re-alignments for them.

Fig. 5 summarizes the pointing measurement results of all the pixels in the five arrays after the pre-alignment, and the results after the re-alignment. The pixels with the small lenses are shown in (a) and those with the large lenses in (b).

To summarize our results, we describe the pointing error distributions using the average (μ) and the standard deviation (σ). The results from the small lenses show a distribution of μ = 0.58 deg and σ = 0.27 deg after the pre-alignment, while for the large lenses we found μ= 0.41 deg and σ = 0.22 deg. After the re-alignment we obtain a pointing error distribution of μ = 0.13 deg and σ = 0.06 deg for the small lenses, while μ = 0.08 deg and σ = 0.03 deg for the large lenses. These results show a clear improvement when compared with the previous ones, with the average pointing (μ) reduced by a factor of 4.5 on for the small lenses and a factor of 5.1 for the large lenses, while the pointing variation (σ) is reduced by a factor of 4.5 and 7.3, respectively. These numbers demonstrate that our method works.

The results of large pointing errors observed from the pre-alignment agree with our expectations from the different pointing error contributions as discussed in section II.A. Because the alignment accuracy of the HEB chip to the lens is similar in both pre-alignment and re-alignment, and because the mixer block parts are found to be within the tolerance, we believe that the pointing error found in the pre-alignment must be dominated by the errors during the lens manufacture. An alternative methodology to achieve an accurate pointing is either to manufacture a perfect lens without any errors or to fully characterize a practical lens, from which one can derive the optical axis position on the back of the lens, to which the HEB chip is aligned. Unfortunately, both approaches require a sub-μm accuracy and are believed to be very challenging.

We also note that for both the pre-alignment and the re-alignment results the large lenses consistently show a lower average (μ) in the pointing error distribution, together with a smaller variation (σ), than what is found for the small lenses. This is expected since the small lenses are more sensitive, by a factor of 2, to any HEB chip misalignment and machining tolerances during the manufacture. In the final results, the average is a factor of 1.6 better, while the standard variation is a factor of 2 better, confirming that it is more challenging to have a high accuracy pointing for a small lens. These results also agree with the simulated beam steering factor between the two types of the lenses discussed in section II.A. Additionally, the previous conclusion indicates that our final results are determined by the re-alignment procedure, which has the same absolute accuracy regardless of the lens size.

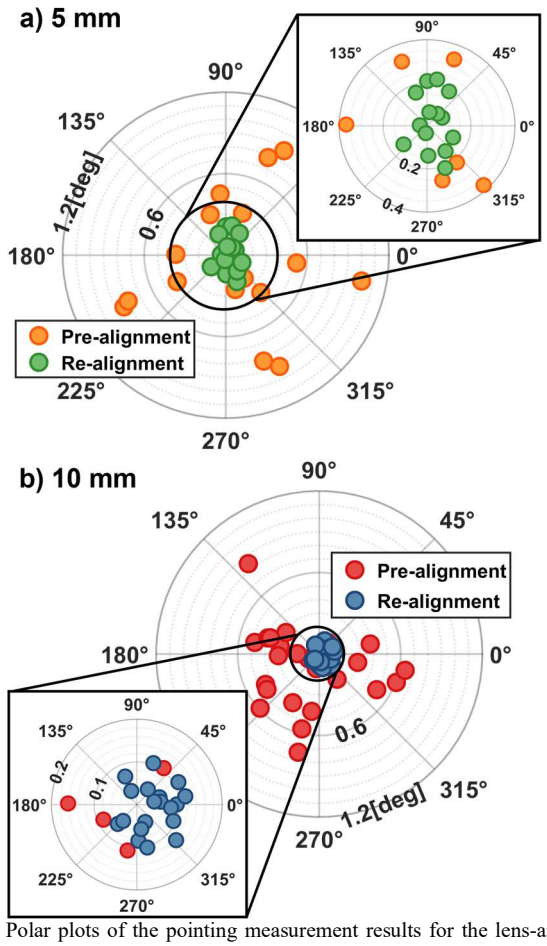

Fig. 5. Polar plots of the pointing measurement results for the lens-antenna mixers in five arrays after pre-alignment and re-alignment. The plots show each pixel pointing error relative to the normal direction of their respective array plane. a) Results for the 5 mm diameter lenses: pre-aligned, in orange, and re-aligned, in green; b) Results for 10 mm diameter lenses: pre-aligned, in red, and re-aligned, in blue.

C. *Re-alignment accuracy*

To further understand the limiting factors of our technique, we take a closer look at the re-alignment data. The zoomed plot in Fig.5(a) indicates that a larger variation in the pointing error occurs in the vertical direction in the case of the small lenses, while for the large lenses, see enlarged plot in Fig. 5(b), the distribution is more uniform and skewed to the right. The different behavior can be attributed to the different circuit board architecture used in the two types of arrays, leading to different orientations of HEB chips. Fig. 6(a) presents the layout of the distribution of the chips for the small lenses, while (b) shows the case for the large lenses. Using the array with the large lenses as an example, there are only two orientations, namely four pixels on either the left or the right side of the array share

This article has been accepted for publication in a future issue of this journal, but has not been fully edited. Content may change prior to final publication. Citation information: DOI 10.1109/TTHZ.2021.3118607, IEEE Transactions on Terahertz Science and Technology

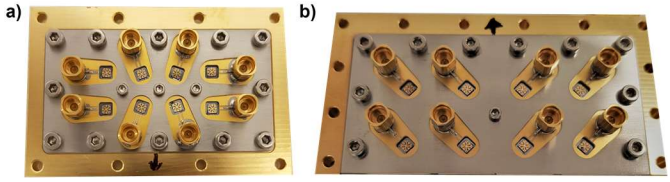

Fig. 6. Back side view of a 4×2 HEB mixer array, where an HEB, IF CPW line, and IF connector for each pixel can be seen. a) array with 5 mm diameter lenses. b) array with 10 mm lenses. It is important to notice the different HEB chip orientations in the two arrays

one orientation. More precisely, they are rotated, 45 degrees towards the left or the right relative to the vertical orientation. The different orientations cause different projections of the re-alignment error in the pointing measurement, leading to the aforementioned results. To characterize the remaining misalignment after the re-alignment we re-applied our methodology to calculate the correction required to have zero pointing error. We found on average a misalignment of 1-2 μm to the right direction relative to the alignment axis, for both types of the arrays. This systematic offset is attributed to our chip gluing process. Furthermore, we found a variation of ± 2μm on the alignments, which indicates the limit of our alignment accuracy.

The results above demonstrate for the first time an unprecedented pointing accuracy for lens-antenna systems at the higher THz frequencies. They are comparable, or even lower, than the results reported for the lens-antenna mixers in HIFI band 6 and 7 mixers [28] for operation up to 1.4 THz, which used auxiliary optics to achieve the instrument's required pointing accuracy. Moreover, our results are also comparable to those achieved in the ALMA band 5 mixers [29] using a feed horn-waveguide coupling scheme. These comparisons clearly show that our technique enables lens-antenna mixers to compete with traditional feedhorn-waveguide mixers, while avoiding the need for extra auxiliary optics, otherwise potentially avoidable, in the instrument optical path.

D. Effect on the coupling to LO

The mixer arrays need to be operated with an array of LOs, namely 8 Gaussian beams, to function as a receiver. To understand the impact of the pointing error on the optical coupling to the LOs, we calculate the power coupling efficiency due to the influence of tilt, K_{tilt}, using (2) which is simplified from [30]

$$K_{tilt} = \exp\left[-2\left(\frac{\theta}{\theta_t}\right)^2\right] \quad (2a)$$

$$\theta_t = \frac{\lambda}{\pi}\sqrt{\frac{2}{w_0^2}} \quad (2b)$$

where θ is the measured pointing error, λ the wavelength of the LOs, and w_0 the lens-antenna beam waist. We assume our lens-antenna beam waists to be the same as their respective LOs, so no mismatch between the beams except for the tilt. We have also characterized the mixer beams using a heterodyne technique. For the large lenses we found a beam waist radius of 3.6 mm and 4 mm operated at 1.9 and 1.4 THz, respectively, while the beam waist for the small lenses was found to be 1.8 mm operated at 4.7 THz. The results however will be published elsewhere [25] since they are beyond the scope of this paper.

We calculate the coupling efficiency based on the μ and the limits of the 1σ range (μ [μ-1σ; μ+1σ]) of the pointing error distribution. Using the re-alignment results, we calculate the coupling efficiency for a mixer array with the small lenses to the respective LO to be 96% [94%;99%], while for an array with the large lenses to be 98% [97%;99%]. A consequence of the application of our technique is that the power distribution within the array is relatively uniform, which is crucial to reach a uniform performance among all the pixels. In contrast, using the pre-aligned results for the array with the small lenses as an example, the coupling efficiency distribution was 45% [17;81%] which is considerably worse. Here, not only the average coupling is low, but also the coupling variation is high. Such a result, together with the fact that there is limited power available from a 4.7 THz LO and also nonuniformity of multi-beams from the Fourier phase grating [12], makes the array receiver impossible to function properly. Therefore, we conclude that the results after realignment have been improved significantly and are also necessary.

E. Pointing results of final arrays

In Fig. 7 and Fig. 8 we summarize the final measured pointing of different pixels in two arrays, together with photos of the two completed arrays. The final pointing results for each pixel in an array with the large lenses are shown in Fig. 7(a) and, those with the small lenses in Fig. 8(a). The front view of the corresponding array is shown in Fig 7(b) and Fig. 8(b), respectively. The pointing direction in Fig. 7 (a) and Fig. 8(a) can be seen as the propagation direction of the light that is "emitted" from the detector at the back of a lens and transmitted through the lens towards the far-field, as seen from the reader perspective.

Our results demonstrate that all the pixels in the array with the large lenses have in principle meet the 0.1 degrees requirement, except for the two pixels, which are maximally 0.02 degrees higher. However, in the array with the small lenses three pixels have met the requirement, while the other five pixels exceed the requirement with a pointing error ranging from 0.13 to 0.21 degrees. Despite of the slightly higher pointing error, these pixels pointing direction is towards the inside of the array, which combined with the uniform coupling to the LO shown in Section III.D meets the condition described in section I where the pointing requirement can be relaxed. Thus, both arrays are considered to satisfy the performance of GUSTO.

This article has been accepted for publication in a future issue of this journal, but has not been fully edited. Content may change prior to final publication. Citation information: DOI 10.1109/TTHZ.2021.3118607, IEEE Transactions on Terahertz Science and Technology

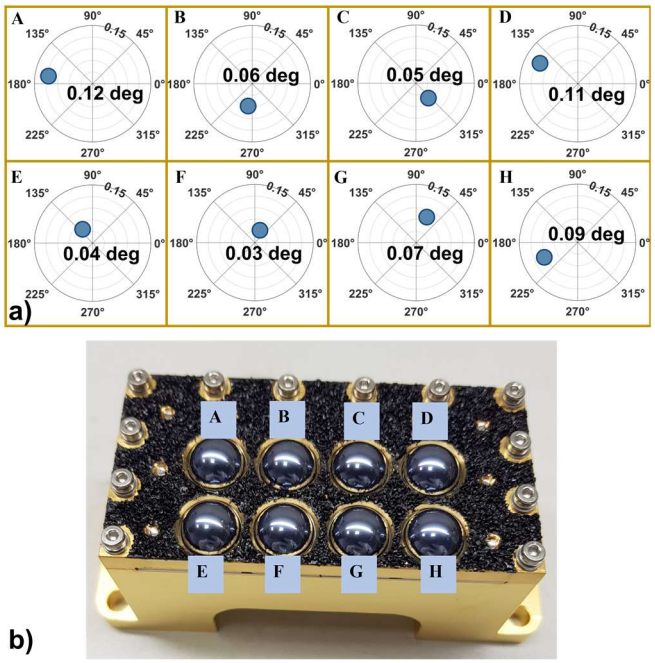

Fig. 7. a) Polar plots summarizing the final pointing error for a re-aligned 4×2 pixel array using the large lenses. The pointing direction is seen as the propagation direction of light that is "emitted" from the detector at the back of a lens and transmitted through the lens towards the far-field, as seen from the reader perspective. B) Front view of the final assembled array. The front of the 8 lenses can be seen, with the 8 HEB detectors assembled on their backside (not visible).

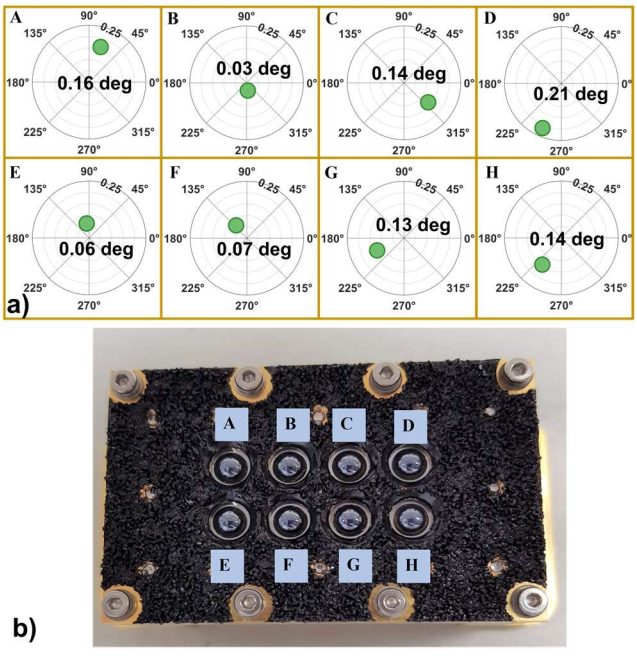

Fig. 8. a) Polar plots summarizing the final pointing error for a re-aligned 4×2 pixel array using the small lenses. The pointing direction is seen as the propagation direction of light that is "emitted" from the detector at the back of a lens and transmitted through the lens towards the far-field, as seen from the reader perspective. b) Front view of the final assembled array. The front of the 8 lenses can be seen, with the 8 HEB detectors assembled on their backside (not visible).

IV. Conclusions

We have for the first time succeeded in demonstrating a technique allowing the lens-antenna, quasi-optical HEB mixers of a 4×2 pixel array to achieve a high accuracy pointing for their far field beams at the high frequencies up to 5.3 THz. Our methodology includes aligning a detector chip to a lens, then determining the pointing error of the beam with respect to the normal direction of the array plane with a high accuracy, and re-aligning the chip to a new position to correct the measured error. Among all re-aligned pixels, we have achieved a final pointing error distribution with an average $\mu = 0.13$ deg and standard deviation $\sigma = 0.06$ deg for 14 pixels out of two arrays using 5 mm diameter lenses, designed for operation at 4.7 THz. We obtained $\mu = 0.08$ deg and $\sigma = 0.03$ deg for 19 pixels out of three arrays using 10 mm diameter lenses, aimed for operation at 1.4 or 1.9 THz. The maximal uncertainty of the pointing measurements is found to be ±0.03 deg. We also found that the re-alignment reduces the pointing error significantly. For example, for the pixels with the large lenses, the average is improved by a factor of 5.1, and the pointing variation is reduced by a factor of 7.3, in comparison with the results from the pre-alignment. Similar improvements are found for the pixels with the small lenses, but less significant, confirming the simulations results, namely it is more challenging to reach high accuracy pointing for the smaller lenses since they are more sensitive to misalignments.

The arrays used for our measurements are the array receivers developed for NASA's balloon borne GUSTO observatory. They show an average coupling efficiency of 96% to the 4×2 Gaussian beams with equal power of an ideal array of LOs at 4.7 THz, and 98% or higher to an array of LOs at 1.4 and 1.9 THz. We also obtain a small variation of the coupling efficiency within an array, which is less than 4% at 4.7 THz as the worst case. Furthermore, the final arrays, as shown in Fig. 7 and Fig. 8, have met the requirement of the GUSTO telescope optics and do not introduce any considerable spillover effect in its secondary mirror.

Our technique demonstrated with the unprecedented pointing accuracy is useful and reliable, enabling highly co-aligned quasi-optical mixers in a focal plane array, with any combination of an antenna and a lens. Moreover, our approach can also be applied to any other incoherent detectors using a lens-antenna coupling scheme, such as the lens-antenna coupled KIDs detectors described in [31], since our HEB is operated in its direct detector mode in this case, and even lens-antenna detectors beyond astronomic applications. Furthermore, our work opens the door for focal-plane arrays using a quasi-optical approach to compete with those based on traditional feedhorn-waveguide.

Appendix A
Lens-Antenna Alignment Protocol

The pre-alignment process starts with marking a few dots near an edge of the back surface of a lens, as illustrated by Fig. A.1(a). It creates an absolute reference for later use during re-alignment. An HEB chip is then placed on the back surface of the lens and positioned using an in-house made alignment unit, which is shown in Fig. A.1(b). The alignment unit is then taped to an Mitutoyo optical microscope stage as shown in Fig.

A.1(c). This stage has a XY movement with 1 μm resolution and a digital readout. The center of the lens is found by finding and recording the horizontal and vertical lens edge positions with the average position for each direction being the coordinates of the lens center. The horizontal edge positions are found when the vertical axis of the microscope crosshair is tangent to the lens edge and vice versa for the vertical direction. The HEB antenna is then aligned to the lens center position, within ±1μm for two orthogonal directions. The HEB is then glued to the lens.

After the pointing measurement, described in section II.C, we derive the required HEB movement relative to the initial position which will correct the existing pointing offset. To calculate the correction, we use the beam steering factor obtained for the respective lens, discussed in section II.A, to convert from degrees to micrometers. Moreover, we also keep track of the relationship between the reference axis used for the pointing measurements and the one used for the HEB realignment, in order to obtain the correct direction of the realignment. To perform the realignment, we need to disassemble the array. Before we remove the chip from the lens, we register the chip orientation relative to the marks on the lens using the microscope. The chip is square, and we chose a side that we can easily identify as reference, then we align the horizontal axis of the crosshair to this side of the chip by rotating the microscope stage. We move the stage in the vertical direction until the marks are seen and register the horizontal axis relation to the marks as shown in Fig. A.1(d). Since the marks are engraved on the lens surface and the picture is based on the microscope image, with the crosshairs overlaid, this acts as an accurate absolute reference. Afterwards, the current X and Y coordinates of the antenna center are measured with respect to the assumed (0,0) position of the lens. The chip is then unglued and detached from the lens with acetone that is applied carefully droplet by droplet on the glue around the chip. Then, we re-align the chip to the new desired position. During the re-alignment we ensure the chip orientation relative to the marks is reproduced. This is crucial because our approach is based on a relative shift of the antenna with respect to its original position.

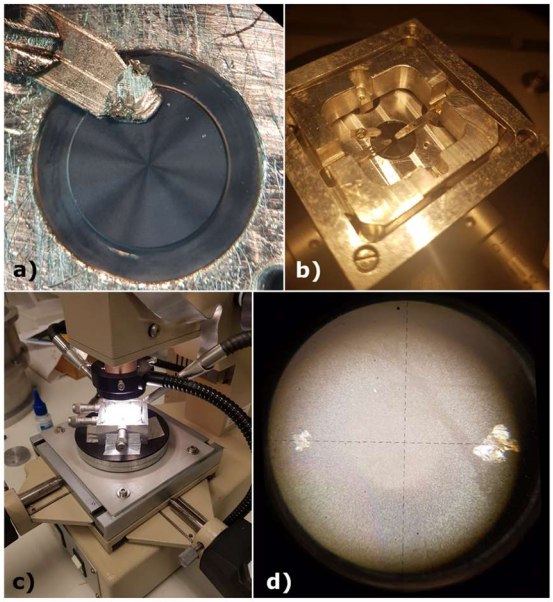

Fig. A.1. Illustration of the alignment method. a) Three small dots engraved on the top right side of the lens as the reference mark. b) In-house made alignment unit to position the HEB chip using two micrometer manipulators, where the HEB chip is pressed down on the back surface of the lens. c) The alignment unit mounted on the XY stage of a microscope. d) Example of a mark reference to register the chip orientation.

ACKNOWLEDGMENT

We acknowledge Nathan Vercruyssen and Behnam Mirzaei for the fabrication and DC tests of the HEB detectors used, and technical support from Jarno Panman, Rob van der Schuur, Erik van der Meer, Henk Ode, Duc Nguyen and Marcel Dijkstra. We thank Jochem Baselmans, Robert Huiting and Sebastian Hähnle for the glow bar setup design. We also thank Ronald Hesper, Stephen Yates, Brian Jackson, Willem Jellema and Vitor Silva for the helpful discussions.

REFERENCES

[1] U. U. Graf, C. E. Honingh, K. Jacobs, and J. Stutzki, "Terahertz Heterodyne Array Receivers for Astronomy," J. Infrared, Millimeter, Terahertz Waves, vol. 36, no. 10, pp. 896–921, 2015.

[2] C. Pabst, R. Higgins, J. R. Goicoechea, D. Teyssier, O. Berne, E. Chambers, M. Wolfire, S. T. Suri, R. Guesten, J. Stutzki, U. U. Graf, C. Risacher, and A. G. G. M. Tielens, "Disruption of the Orion molecular core 1 by wind from the massive star θ1 Orionis C," Nature, vol. 565, no. 7741, pp. 618–621, 2019.

[3] Y. M. Seo, P. F. Goldsmith, C. Walker, D. J. Hollenbach, M. G. Wolfire, C. Kulesa, V. Tolls, P. N. Bernasconi, Ü. Kavak, F. F. S. van der Tak, R. Shipman, J. R. Gao, A. Tielens, M.G. Burton, H. York, E. Young, W. L. Peters, A. Young, C. Groppi, K. Davis, J. L. Pineda, W. D. Langer, J. H. Kawamura, A. Stark, G. Melnick, D. Rebolledo, G. F. Wong, S. Horiuchi and T. B. Kuiper "Probing ISM Structure in Trumpler 14 and Carina I Using the Stratospheric Terahertz Observatory 2," Astrophys. J., vol. 878, no. 2, 2019.

[4] The Event Horizon Telescope Collaboration, "First M87 Event Horizon Telescope Results. I. The Shadow of the Supermassive Black Hole", Astrophys. J. L., vol. 875, 2019.

[5] C. K. Walker, "THz Coherent Detection Systems", in Terahertz Astronomy, 1st ed., FL, USA: Taylor &Francis, 2016, pp159–227.

[6] J. V. Siles, R. H. Lin, C. Lee, E. Schlecht, A. Maestrini, P. Bruneau, A. Peralta, J. Kloosterman, J. Kawamura and I. Mehdi, "Development of High-Power Multi-Pixel LO Sources at 1.47 THz and 1.9 THz for Astrophysics: Present and Future", Proc. 26th International Symposium on Space Terahertz Technology, Cambridge, MA, USA, 2015, pp 40-42.

[7] M. S. Vitiello, G. Scalari, B. Williams, and P. De Natale, "Quantum cascade lasers: 20 years of challenges", Optics Express, vol.23, no. 4, pp.5167–5182, 2015.

[8] B. S. Williams, "Terahertz quantum-cascade lasers", Nat. Photonics, vol. 1, pp.517–525, 2007.

[9] W. Zhang, P. Khosropanah, J. R. Gao, E. L. Kollberg, K. S. Yngvesson, T. Bansal, R. Barends and T. M. Klapwijk, "Quantum noise in a terahertz hot electron bolometer mixer", Appl. Phys. Lett., Vol. 96, no. 11, pp. 11–13, 2010.

[10] A. Khalatpour, J. L. Reno, N. P. Kherani, and Q. Hu, "Unidirectional photonic wire laser," Nat. Photonics, vol. 11, no. 9, pp. 555-559, 2017.

[11] A. Khalatpour, J. L. Reno, and Q. Hu, "Phase-locked photonic wire lasers by π coupling," Nat. Photonics, vol. 13, no.1, pp. 47-53, 2019.

[12] B. Mirzaei, Y. Gan, M. Finkel, C. Groppi, A. Young, C. Walker, Q. Hu, J. L. Reno, and J. R. Gao, "4.7 THz asymmetric beam multiplexer for GUSTO," Opt. Express, vol. 29, no. 15, pp. 24434–24445, 2021.

[13] C. Risacher, R. Gusten, J. Stutzki, H. Hubers, D. Buchel, U. U. Graf, S. Heyminck, C. E. Honingh, K. Jacobs, B. Klein, T. Klein, C. Leinz, P. Pütz, N. Reyes, O. Ricken, H. Wunsch, P. Fusco, and S. Rosner, "First Supra-THz Heterodyne Array Receivers for Astronomy with the SOFIA Observatory," IEEE Trans. Terahertz Sci. Technol., vol. 6, no. 2, pp. 199–211, 2016.

[14] C. Walker, C. Kulesa, P. Bernasconi, H. Eaton, N. Rolander, C. Groppi, J. Kloosterman, T. Cottam, D. Lesser, C. Martin, A. Stark, D. Neufeld, C. Lisse, D. Hollenbach, J. Kawamura, P. Goldsmith, W. Langer, H. Yorke,

J. Sterne, A. Skalare, I. Medhi, S. Weinreb, J. Kooi, J. Stutzski, U. Graf, M. Brasse, C. Honingh, R. Simon, M. Akyilmaz, P. Puetz and Mark Wolfire, "The Stratospheric THz Observatory (STO)," in Proc. SPIE, Millimeter, Submillimeter, and Far-Infrared Detectors and Instrumentation of Astronomy VII, Austin, TX, USA, vol. 7733, 2010, paper 77330N-1.

[15] J. R. G. Silva, B. Mirzaei, W. Laauwen, N. More, A. Young, C. Kulesa, C. Walker, A. Khalatpour, Q. Hu, C. Groppi, J. R. Gao, "4×2 HEB receiver at 4.7 THz for GUSTO," in Proc. SPIE, Millimeter, Submillimeter, and Far-Infrared Detectors and Instrumentation of Astronomy VII, Austin, TX, USA, vol. 10708, 2018, paper 107080Z.

[16] OASIS - "Orbiting Astronomical Satellite Investigating Stellar Systems". A mission concept to be proposed to NASA to respond to the Astrophysics Medium Explorers (MIDEX) Announcement of Opportunity (AO). Expected to be released fall of 2021.

[17] P. Putz, K. Jacobs, M. Schultz, M. Justen, R. Higgings, S. Fathi, C. E. Honingh and J. Stutzki, "HEB Waveguide Mixers for the upGreat 4.7 THz Heterodyne Receiver Array", Proc. 27th International Symposium on Space Terahertz Technology, Nanjing, China, 2016.

[18] P. Pütz, C. E. Honingh, K. Jacobs, M. Justen, M. Schultz, and J. Stutzki, "Terahertz hot electron bolometer waveguide mixers for GREAT," Astron. Astrophys., vol. 542, 2012.

[19] S. Cherednichenko, V. Drakinskiy, T. Berg, P. Khosropanah and E. Kollberg, "Hot-electron bolometer terahertz mixers for the Herschel Space Observatory", Review of Sci. Instruments, vol. 79, pp.3, no. 034501, 2008.

[20] B. D. Jackson, "NbTiN-Based THz SIS Mixers for the Herschel Space Observatory", PhD dissertation, Fac. of App. Sci., TU Delft, NL, 2005.

[21] P. Khosropanah, J. R. Gao, W. M. Laauwen and M. Hajenius, "Low noise NBN hot electron bolometer mixer at 4.3 THz", Appl. Phys. Lett., vol. 91, no. 221111, 2007.

[22] The spiral antenna design parameters are: starting radius, k =4μm; curvature, a=0.318; arm width, δ=83deg.

[23] D.F. Filipovic, S. S. Geahart and G. M. Rebeiz, "Double-slot Antennas on Extended Hemispherical and Elliptical Silicon Dielectric Lenses," IEEE Trans. Microwave. Theory Tech., vol. 41, no. 10, pp. 1738–1749, 1993

[24] HFSS: www.ansys.com

[25] J. R. G. Silva, M. Finkel, W. M. Laauwen, S. Yates, B. Mirzaei, N. Vercruyssen. A. Young, C. Kulesa, F. van der Tak, J. R. Gao, "Gaussicity and beam waist properties of spiral antenna coupled HEB mixers at supra-THz" (in preparation).

[26] S. Hähnle, O. Yurduseven, S. Berkel, N. Llombart, J. Bueno, S. Yates, V. Murugesan, D. Thoen, A. Neto and J. Baselmans, "An Ultrawideband Leaky Lens Antenna for Broadband Spectroscopic Imaging Applications" IEEE Trans. Antennas and Propagation, vol. 68, no. 7, pp. 5675-5679, 2020.

[27] Credits: Theodolite 3D model was retrieved from SketchUp 3DWarehouse.

[28] W. Jellema, "Optical Design and Performance Verification of Herschel-HIFI, PhD dissertation, Univ. Groningen, Groningen, NL, 2015.

[29] V. Belitsky, M. Bylund, V. Desmaris, A. Ermakov, S.-E. Ferm, M. Fredrixon, S. Krause, I. Lapkin, D. Meledin, A. Pavolotsky, H. Rashid, S. Shafiee, M. Strandberg, E. Sundin, P. Y. Aghdam, R. Hesper, J. Barkhof, M. E. Bekema, J. Adema, R. de Haan, A. Koops, W. Boland, P. Yagoubov, G. Marconi, G. Siringo, E. Humphreys, G. H. Tan, R. Laing, L. Testi, T. Mroczkowski, W. Wild, K. S. Saini and E. Bryerton, "ALMA Band 5 receiver cartridge Design, performance, and commissioning," Astron. Astrophys. , vol. 98, pp. 1–10, 2018.

[30] P. F. Goldsmith, "Gaussian Beam Coupling", in Quasioptical Systems: Gaussian Beam Quasioptical Propagation and Applications, New York, NW, USA: IEEE Press, 1998, pp. 59-68.

[31] A. Endo, K. Karats, Y. Tamura, T. Oshima, A. Taniguchi, T. Takekoshi, S. Asayama T.J.L. C. Bakx, S. Bosma, J. Bueno, K. W. Chin, Y. Fujii, K. Fujita, R. Huiting, S. Ikarashi, T. Ishida, S. Ishii, R. Kawabe, T. M. Klapwijk, K. Kohno, A. Kouchi, N. Llombart, J. Maekawa, V. Murugesan, S. Nakatsubo, M. Naruse, K. Ohtawara, A. P. Laguna, J. Suzuki, K. Suzuki, D. J. Thoen, T. Tsukagoshi, Te. Ueda, P. J. de Visser, P. P. van der Werf, S. J. C. Yates, Y. Yoshimura, O. Yurduseven and J. Baselmans, "First light demonstration of the integrated superconducting spectrometer", Nat. Astron., vol. 3, pp. 989-996, 2019.